Insight into the structural and optoelectronic properties of e-beam evaporated nanostructured TiO_2 thin films annealed in air

Abdul Faheem Khan[1], Mazhar Mehmood[1], A. M. Rana[2], M. Ashraf[3], A. Mahmood[4], S.K. Durrani[5]

[1]National Centre for Nanotechnology & Department of Chemical and Materials Engineering, Pakistan Institute of Engineering and Applied Sciences (PIEAS), Islamabad 45650 , Pakistan.

[2]Department of Physics, Bahauddin Zakariya University, Multan 60800, Pakistan

[3]Optics Laboratories, P. O. Nilore, Islamabad, Pakistan.

[4]NILOP, Islamabad 45650, Pakistan

[5]P.O. Nilore, Materials Division, PINSTECH

corresponding author (M. Mehmood): mazhar@pieas.edu.pk, Phone: +92-51-2207813, Fax: +92-51-2208070; (A.F. Khan) faheem_khan_1977@yahoo.com

Abstract

About 480 nm thick titanium oxide (TiO_2) thin films have been deposited by electron beam evaporation followed by annealing in air at 300—600^oC with a step of 100^oC for a period of two hours. Optical, electrical and structural properties are studied as a function of annealing temperature. All the films are crystalline (having tetragonal anatase structure) with small amount of amorphous phase. Crystallinity of the films improves with annealing at elevated temperatures. XRD and FESEM results suggest that the films are composed of nanoparticles of 25-35 nm. Raman analysis and optical measurements suggest quantum confinement effects since Raman peaks of the as-deposited films are blue-shifted as compared to those for bulk TiO_2. Optical band gap energy of the as-deposited TiO_2 film is 3.21 eV, which decreases to about 3.06 eV after annealing at 600 ^oC. Refractive index of the as-deposited TiO_2 film is 2.26, which increases to about 2.32 after annealing at 600 ^oC. However the films annealed at 500 ^oC represent peculiar

behavior as its band gap increases to highest value of 3.24 eV whereas refractive index, RMS roughness and dc-resistance illustrate a drop as compared to all other films. Illumination to sunlight decreases the dc-resistance of the as-deposited and annealed films as compared to dark measurements possibly due to charge carrier enhancement by photon absorption.

Keywords: *Nanostructured TiO_2 thin films, quantum confinement, Raman spectroscopy, band gap energy, impedance spectroscopy, and atomic force microscopy.*

1. Introduction

Among the transition-metal oxides, TiO_2 is one of the most extensively studied materials. The rising interest in its applications and research in the last few years is due to its unique and outstanding structural, optical and electronic properties [1-4]. TiO_2 is known to exist in three polymorphic forms: anatase, rutile and brookite. The most widely used crystallographic structures (tetragonal) are anatase and rutile. Depending on the structure, the properties of TiO_2 vary greatly, which make them useful for many applications. The rutile phase has a direct band gap at 3.06 eV and indirect band gap at 3.10 eV [5] with high refractive index and dielectric constant (~ 80) [6,7], better thermal and chemical stability etc. Owning to such properties, the rutile phase has found applications in optical coatings, solar energy converters, storage capacitors in dynamic random access memories (DRAM), as protective layers and as dielectric layer in microelectronic applications [8-10]. On the other hand, the anatase phase exhibits direct band gap ranging from 3.77 to 3.85 eV [11] and the indirect band gap at 3.23 eV with relatively low refractive index and dielectric constant (~ 12-30) [12]. Due to its large

band gap, TiO_2 covers only the UV range of the solar spectrum. The unique properties of anatase phase make it a candidate material for gas sensors, solar cells, dielectrics in semiconducting FETs, self-cleaning windows, anti-fogging glasses, self-sterilizing, and photo-catalytic applications [13, 14]. Contrary to crystalline phase, amorphous TiO_2 with high refractive index demonstrate optical isotropy and high packing density making them suitable for optical applications [8, 15]. Because of successful applications among various fields, nanostructured TiO_2 thin films have attracted tremendous attention due to their quantum confinement effects. Such nanostructured films are considered to be promising host materials as they possess high surface area, chemical stability, good semiconducting properties and low cost [16].

Electrical resistance of TiO_2 is known to alter substantially by introducing oxygen defects leading to its semiconducting behavior [11]. TiO_2 can be used as an electrode for high electron injection as well as multi-layered structures in photovoltaic devices to provide direct electrical pathway for photogenerated electrons to increase the rate of electron transport, which leads to a higher efficiency [17, 18].

TiO_2 thin films have been prepared by many techniques such as chemical vapor deposition [19], sputtering [1, 20], sol-gel [3, 21], pulsed laser deposition [22], plasma oxidation [23] etc. Electron beam evaporation provides large area, high quality films with high volume deposition rates and good adhesion to substrate and purity. In addition, the process parameters like deposition rate and thickness can be easily controlled.

In this paper structural, optical and electrical properties of e-beam evaporated nanostructured TiO_2 thin films have been investigated in pre- and post-thermal annealed (in air over the temperature range of 300–600 ^{o}C) conditions using X-ray diffraction

(XRD), Raman spectroscopy, transmission spectroscopy, impedance spectroscopy (IS), field emission scanning electron microscopy (FESEM), and atomic force microscopy (AFM).

2. Experimental

TiO_2 thin films were deposited using electron beam evaporation of TiO_2 powder (99.99%) as a starting material onto BK7 glass substrates using tungsten crucible. The system was pumped to a base pressure of less than 10^{-5} mbar before deposition and O_2 was injected into the chamber during evaporation at a partial pressure below 2×10^{-4} mbar. The substrate was set at a temperature of 300^{o}C and at a distance of 35 cm from the source and rotated at 30 RPM during deposition to obtain uniform and homogeneous films. The deposition parameters were optimized to reduce the film roughness. Thickness of film and rate of its deposition were controlled with the help of an *in situ* quartz crystal thickness monitor. Intended thickness of the film was about 500 nm and the deposition rate was set at 0.45 nm s^{-1}. However, the thickness estimated by ellipsometery is found to be 480 ± 10 nm, and is considered to be more reliable.

These e-beam deposited films were then annealed in air at various temperatures ranging from 300−600^{o}C with a step of 100^{o}C for a fixed time of 2 h. Structure of these films was determined by recording X-ray diffraction (XRD) patterns at room temperature before and after thermal annealing using Bruker D8 Discover diffractometer equipped with Cu K_α radiations. The Raman spectra were obtained at room temperature using confocal mode of Micro-Raman-Spectrometer (MST-1000A, DongWoo Optron Co. LTD, South Korea) under excitation with HeCd laser beam at 442 nm. Optical transmittance and reflectance of the as-deposited and annealed films were recorded at

room temperature by a Perkin Elmer UV/VIS/NIR Lambda 19 spectrophotometer in the wavelength range 200–2500 nm. Impedance spectroscopic (IS) measurements were made at room temperature using Alpha-A High Performance Frequency Analyzer, Novocontrol Technologies, Germany in the frequency range of 0.1 Hz to 1MHz. Silver paint electrodes were used at a separation of about 15 mm on 25 mm wide films. The contacts were allowed to dry for 24 h in open air before making measurements. Surface morphology of the films was investigated by FESEM (JSM7500F, JEOL, Japan), and atomic force microscopy (Quesant Universal SPM, Ambios Technology) in non-contact mode. An AFM tip of silicon nitride was used having an approximate radius of curvature of 10 nm.

3. Results and Discussion

TiO_2 thin films deposited on BK7 glass substrates are almost free from pinholes and physically stable. Cracks and blisters are not found even after annealing up to 600^{o}C. Fig. 1 shows XRD patterns of the as-deposited and annealed TiO_2 films. As-deposited and annealed films are polycrystalline having anatase tetragonal structure (I41/amd (141)) [24]. Weak intensity and broadness of diffraction peaks for the as-deposited film suggest the presence of some amorphous phase. Crystallinity of the films seems to improve with the rise of annealing temperature as confirmed by the sharpness and intensity of the diffraction peaks. X-ray diffraction peaks are relatively broad signifying that the present films are composed of small nanoparticles [25-28]. The temperature dependence of XRD patterns can be explained primarily by the mobility of atomic species in thin films at various annealing temperatures. At low annealing temperature, the

evaporated species possess small energy and hence a low surface mobility causing a less ordered surface structure. The low mobility of atoms prevents full crystallization of the films. However on annealing at high temperature, atoms acquire high enough mobility to organize themselves in a more crystalline arrangement [29]. The average particle size as estimated from planes with orientations (101) and (004) using Scherrer formula [26] is in the range of 20 nm to 28 nm and demonstrates an improvement with annealing temperature as clear from Fig. 2. Also included in Fig. 2 is the change in unit cell volume with annealing temperature. Furthermore, the unit cell volume of as-deposited and annealed films is found to be slightly greater than that for bulk TiO_2 (0.1363 nm^3).

Fig. 3 shows FESEM images of the as-deposited TiO_2 films. Images of the as-deposited film depict crystalline nature of TiO_2 with small amount of amorphous phase. It has been noticed that the as-deposited film shows the presence of TiO_2 nanocrystals, which appear as spherical clusters and their agglomerates. The average particle size lies in the range of 25 – 35 nm, which is slightly larger than that obtained from the XRD results. The agreement in the XRD and FESEM data can be made by keeping in view the fact that smaller primary particles have a large surface free energy and would, therefore, tend to agglomerate faster and grow into larger grains [1].

Two and three-dimensional AFM images of the as-deposited, 300ºC and 600ºC annealed TiO_2 films are shown in Fig. 4. It can be seen that all the films are crystalline with some amount of amorphous phase. The crystallinity of the films improves with the rise of annealing temperature as observed from Fig. 4. The surface asperities and depressions are of the order of 25-35 nm wide. RMS roughness of the as-deposited film is about 26 nm, which increases to about 36 nm on annealing except at 500^{o}C where it

decreases to about 28 nm as clear from the inset of Fig. 4, representing non-uniform growth. This is also confirmed from the height scales of 2D AFM images.

Another very useful tool to distinguish between various crystalline phases of TiO_2 thin films is the Raman spectroscopy. The anatase phase of TiO_2 is known to comprise of six atoms per unit cell (with space group $\mathbf{D}_{4h}^{19}$) giving 15 vibrations modes. Among these optical modes A_{2u}, B_{2u}, E_u are IR active while A_{1g}, B_{1g}, E_g modes at 144, 197, 399, 515, 519 and 639 cm^{-1} are Raman active [14, 17, 30]. The intensity and shape of IR and/or Raman peaks show variations with microstructure, particle shape, size and defects. Fig. 5 shows Raman spectra of the as-deposited and annealed TiO_2 films. The frequencies for various vibration modes were recognized by applying a Gaussian peak fit analysis. Three Raman peaks are visible in the spectrum of as-deposited film at about 394, 512 and 630 cm^{-1} and are assigned to B_{1g}, $A_{1g} + B_{1g}$ and E_g optical phonons respectively [14, 17] and no Raman peak for the rutile phase has been noted. These Raman peaks are blue-shifted as compared to those for bulk TiO_2 (399, 515 and 639 cm^{-1}) [30], suggesting quantum confinement effects. These Raman peaks remain unaffected up to annealing temperature of 400°C. But the peak at 394 cm^{-1} corresponding to B_{1g} mode show more blue-shift on annealing at higher temperatures. While peaks at 512 and 630 cm^{-1} corresponding to A_{1g}+B_{1g} and E_g modes show a red-shift on annealing at higher temperatures, possibly caused by the grain growth and orderedness. The deviation of Raman peaks may also be due to non-stoichiometry of the TiO_2 [25]. Intensity of the Raman peaks shows slight increase with annealing temperature due to improvement in the structural order. The asymmetry of the Raman peaks may be attributed to small size of nanoparticles and structural defects [25, 26].

Fig. 6 shows plot of transmittance of the as-deposited and annealed TiO_2 films at different temperatures as a function of wavelength. An almost similar behavior of transmittance is observed for all the films in the wavelength range of 300-3000 nm with a slight shift in the peak position towards higher wavelengths. Ripples in the transmittance spectra are a consequence of the light interference [11]. The blunt and slow decrease below 500 nm probably due to the absorption edge manifests the presence of amorphous phase in the as-deposited film as observed by XRD and FESEM. Factors like non-stoichiometry, orderedness, residual stresses and defects formed during film deposition may cause observed variations in the transmittance.

Fig. 7 is a plot of absorption coefficient α as a function of photon energy, $h\nu$, for the determination of band gap. Band gap energy, E_{opt}, values estimated by extrapolating α–$h\nu$ plots of Fig. 7 are portrayed in Fig. 8 as a function of annealing temperature. Optical band gap values of the TiO_2 films show almost a decreasing trend with a substantial fall from 3.21 eV (for the as-deposited film) to 3.06 eV except for the film annealed at 500°C which indicates a rise of E_{opt} value to 3.24 eV. These E_{opt} values are almost in agreement with the indirect band gap value (3.23 eV [12]) of TiO_2 films. The lowest value of E_{opt} for the film annealed at 600°C matches with the direct forbidden band gap value of 3.03 eV [14]. This forbidden gap seems to be generated with an indirect allowed transition [31], but as the direct forbidden transitions are weaker in strength, the indirect allowed transitions play a dominant role in the optical absorption [14]. The decreasing behavior of E_{opt} values with annealing has also been observed by Karunagaran *et al*. [14] and Radecka *et al*. [32]. Such variations in the E_{opt} values could

be associated with the structural modifications as seen in Raman studies (Fig. 5), and/or rise in crystallite size as observed in XRD (Figs. 1,2).

Fig. 9 shows reflectance, *R*, of the as-deposited and annealed films as a function of wavelength. An almost similar trend is observed for all films with a slight shift of peaks towards lower wavelengths up to an annealing temperature of 400ºC but above this temperature peaks shift slightly towards higher wavelengths. It might be caused by structural modifications as observed in Raman and AFM studies. Transmittance data can be employed to determine refractive index, *n,* using the relations described elsewhere [25]. Fig. 10 depicts refractive index (calculated at λ=550 nm) as a function of annealing temperature (T_A). The refractive index is found to increase from 2.26 to 2.32 except for the film annealed at 500°C which shows the lowest value of 2.1. Refractive index reported for crystalline anatase TiO_2 thin film is 2.40 and for the anatase single crystal is 2.50 [33]. Present values of refractive index are slightly lower than the reported anatase values. The low value of refractive index could seem to be due to partial crystallinity and low adatom mobility of the films at room temperature. It has been noticed that the refractive index and band gap energy show opposite trend with annealing. Such type of behavior has also been noticed by Ali *et al* [34].

Impedance spectroscopy is a useful tool for the characterization of intrinsic electrical properties of a material. Fig. 11 represents a typical complex impedance spectrum (Z'' plotted against Z') for the as-deposited TiO_2 film recorded at room temperature while illuminating the film to the sunlight as well as keeping it in the dark. Such impedance spectra for all the annealed films show single depressed semicircles (not shown here) analogous to that of the as-deposited film for both types of measurements.

The depressed semicircles are caused by the distribution of relaxation time showing the non-Debye nature of the films [35]. Measured data is well fitted with the simulated curve using an equivalent RC parallel circuit (shown as inset of Fig. 11). The dc resistance can be determined from the intercept on Z'-axis in the fitted Nyquist plot (Fig. 11). Optimum (best-fitted) value of capacitance, C_1, is found to be approximately same for all the films and is about 50 pF. In contrast, optimum value of dc-resistance, R_1, indicates an increasing performance (2.8-10.3 x 10^9 Ω) with rise of annealing temperature except for the film annealed at 500°C which shows a decrease to 4.25 x 10^9 Ω for the measurements made in the dark as obvious from Fig. 12. This behavior of R_1 is in-line with those of refractive index and RMS roughness but opposite with that of optical band gap (Figs. 4, 8, 10, 12). Measured resistances and capacitances may be a characteristic of grain boundaries between nanocrystals [28,36]. The fall of dc resistance (Fig. 12) seems to be a consequence of the structural modifications of the film, whereas the rise of resistance may be related with the reduction of carrier density through trapping of electrons at grain boundaries by adsorbed oxygens [36] during annealing in air. It is also notable from Fig. 12 that the dc-resistance is low when the measurements were made in sunlight as compared to those measured in the dark. It is an indicative for the rise of charge carrier density due to the absorption of photons.

4. Conclusions

The e-beam evaporated TiO_2 thin films are crystalline in nature possessing the anatase structure along with some amorphous phase. The amorphous phase reduces and improves crystalline character of the films with annealing at high temperatures. The post thermal annealing demonstrates greater affinity to alter the structural and optoelectronic

properties of TiO_2 thin films which contain nanoparticles of size 25-35 nm. Raman spectrum of as-deposited TiO_2 film is blue-shifted indicating nanostructure and quantum confinement effects. Due to such quantum confinement effects and structural adjustments band gap energy of TiO_2 decreases from 3.21 eV to 3.06 eV, whereas an increase in refractive index, RMS roughness and dc-resistance has been noticed. The film annealed at 500 ^oC represents peculiar behavior as band gap increases to highest value of 3.24 eV whereas refractive index decreases to lowest value of 2.1 as well as RMS roughness and dc-resistance show a drop as compared to other films. The films reveal lower resistance if illuminated to sunlight in comparison with measurements in the dark caused by increase in charge carriers by the absorption of photons.

Acknowledgement

Authors are thankful to Higher Education Commission (HEC), Government of Pakistan, for financial support.

References

[1] P. Singh, A. Kumar, D. Kaur, Physica B 403 (2008) 3769.

[2] G.W. Lee, J.H. Byeon, Mater. Char. 60 (2009) 1476.

[3] D. Crisan, N. Dragan, M. Crisan, M. Raileanu, A. Braileanu, M. Anastasescu, A. Lanculescu, D. Mardare, D. Luca, V. Marinescu, A. Moldovan, J. Phys. Chem. Solids 69 (2008) 2548.

[4] S. Murugesam, P. Kuppusami, E. Mohandas, Mater. Res. Bull. 45 (2010) 6.

[5] A. Welte, C. Waldauf, C. Brabec, P.J. Wellmann, Thin Solid Films 516 (2008) 7256.

[6] P. Chowdhury, H.C. Barshilia, N Selvakumar, B. Deepthi, K.S. Rajam, A.R. Chaudhuri, S.B. Krupanidhi, Physica B, 403 (2008) 3718.

[7] G.D. Wilk, R.M. Wallace, J.M. Anthony, J. Appl. Phys. 89 (2001) 5243.

[8] A. Bendavid, P.J. Martin, E.W. Preston, Thin Solid Films 517 (2008) 494.

[9] R. Sikora, J. Phys. Chem. Solids 66 (2005) 1069.

[10] J.Y. Gan, Y.C. Chang, T.B. Wu, Appl. Phys. Lett. 72 (1998) 332.

[11] C. Yang, H. Fan, Y. Xi, J. Chen, Z. Li, Appl. Surf. Sci. 254 (2008) 2685.

[12] M. Kadoshima, M. Hiratani, Y. Shimamoto, K. Torii, H. Miki, S. Kimura, T. Nabatame, Thin Solid Films 424 (2003) 224.

[13] M. Maeda, T. Watanabe, Surf. Coat. Technol. 201 (2007) 9309.

[14] B. Karunagaran, K. Kim, D. Mangalaraj, J. Yi, S. Velumani, Sol. Energy Mater. Sol. Cells 88 (2005) 199.

[15] B.K. Tay, Z.W. Zhao, D.H.C. Chua, Mater. Sci. Engg. R52 (2006) 1.

[16] G.H Du, Q. Chen, R.C. Che, Z.Y. Yuan, L.M. Peng, Appl. Phys. Lett. 79 (2001) 22.

[17] X. Dong, J. Tao, Y. Li, H. Zhu, Appl. Surf. Sci. doi: 10.1016/j.apsusc.2009.10.100.

[18] L.H. Chong, K. Mallik, C.H. de Groot, R. Kersting, J. Phys: Condens. Matter. 18 (2006) 645.

[19] V.G. Besserguenev, R.J.F. Pereira, M.C. Mateus, I.V. Khmelinskii, R.C.Nicula, E. Burkel, Int. J. Photoenergy 5 (2) (2003) 99.

[20] L.J. Meng, V. Teixeira, H.N. Cui, F. Placido, Z. Xu, M.P. dos Santo, Appl. Surf. Sci. 252 (2006) 7970.

[21] G. Facchin, G. Carturan, R. Campostrini, S. Gialanella, L. Lutterotti, L. Armeleo, G. Marci, L. Palmisano, A. Sclafani, J. Sol-Gel Sci. Technol. 18 (2000) 29.

[22] A. De Giacomo, O. De Pascale, Appl. Phys. A 79 (4–6) (2004) 1405.

[23] J.C. Tinco, M. Estrada,G. Romero, Microelectron. Reliab. 43 (2005) 895.

[24] The Joint Committee on Powder Diffraction Standards (JCPDS), Card No. 89-4921, International Centre for Diffraction Data (ICDD), Swarthmore, PA, USA.

[25] A.F. Khan, M. Mehmood, A.M. Rana, M.T. Bhatti, A. Mahmood, Chin. Phys. Lett. 7 (2009) 077803.

[26] A.F. Khan, M. Mehmood, A.M. Rana, M.T. Bhatti, Appl. Surf. Sci. **255** (2009) 8562.

[27] A.F. Khan, M. Mehmood, A.M. Rana, T. Muhammad, Appl. Surf. Sci. (2009), doi:10.1016/j.apsusc.2009.09.043.

[28] A.F. Khan, M. Mehmood, M. Aslam, M. Ashraf, Appl. Surf. Sci. (2009), doi:10.1016/j.apsusc.2009.10.047.

[29] H.R. Fallah, M. Ghasemi, A. Hassanzadeh, Physica E 39 (2007) 69.

[30] J. Zhang, M.J. Li, Z.C. Feng, J. Chen, C. Li, J. Phys. Chem. B 110 (2006), 927.

[31] K.M. Glassford, J.R. Chelikowsky, Phys. Rev. B 46 (1992) 1284.

[32] M. Radecka, K.Z. Akrzewska, H. Czternastek, T. Stapinski, S. Debrus, Appl. Surf. Sci. 65/66 (1993) 227.

[33] M. Lazzeri, A. Vittabine, A. Selloni, Phys. Rev. B 65 (2002) 119901.

[34] H.M. Ali, M.M. Abou-Mesalan, M.M. El-Shorbagy, J. Phys. Chem. Solids 71 (2010) 51.

[35] A.F. Khan, M. Mehmood, M. Aslam, S.I. Shah, J. Colloid Interface Sci. (2009), doi:10.1016/j.jcis.2009.11.045.

[36] W. Göpel, K.D. Schierbaum, Sens. Actuators B 26–27 (1995) 1.

Captions

Fig.1. X-ray diffraction patterns of TiO_2 thin films, as-deposited (a) and annealed for 2hrs at 300 ^oC (b), 400 ^oC (c), 500 ^oC (d), and 600 ^oC (e).

Fig.2. Plots of volume of the unit cell (*curve 1*) and particle size (*curve 2*) as a function of annealing temperature (T_A) for TiO_2 thin films.

Fig.3. FESEM images of the as-deposited TiO_2 thin films.

Fig.4. AFM images (1000 x 1000 nm^2) showing the surface morphology of TiO_2 thin film annealed at 350^oC for 2 hrs. The inset represents plot of RMS roughness vs. annealing temperature (T_A).

Fig.5. Raman Spectra of TiO_2 thin films at various annealing temperatures.

Fig.6. Optical transmittance of TiO_2 thin films, as-deposited (a) and annealed for 2hrs at 300 ^oC (b), 400 ^oC (c), 500 ^oC (d), and 600 ^oC (e).

Fig.7. Plots of α vs. photon energy, $h\nu$, for TiO_2 thin films at various annealing temperatures.

Fig.8. Plot of optical band gap, E_{opt}, vs. annealing temperature, T_A, for TiO_2 thin films.

Fig.9. Optical reflectance of TiO_2 films as a function of wavelength at various annealing temperatures.

Fig.10. Plots of refractive index, *n,* vs. annealing temperature, T_A, for TiO_2 thin films at wavelength λ = 550 nm.

Fig.11. Nyquist plots of as-deposited TiO_2 thin film along with fitted data using equivalent circuit as shown.

Fig.12. Plot of dc-resistance vs. annealing temperature, T_A, for TiO_2 thin films.

Fig. 1

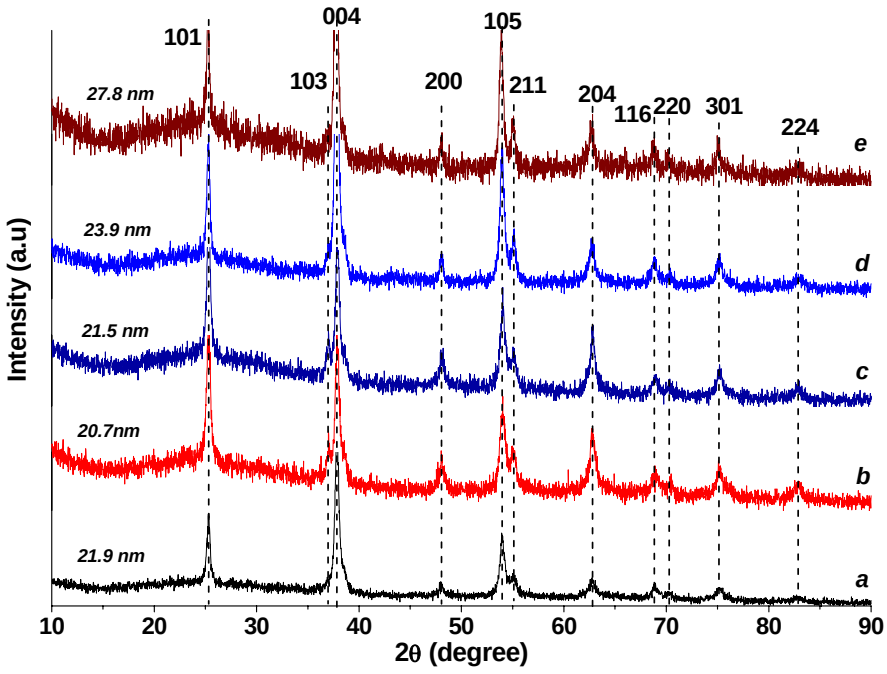
101
004
105
103
200
211
204
116
220
301
224
27.8 nm
23.9 nm
21.5 nm
20.7nm
21.9 nm
e
d
c
b
a
Intensity (a.u)
10
20
30
40
50
60
70
80
90
2θ (degree)

Fig. 2

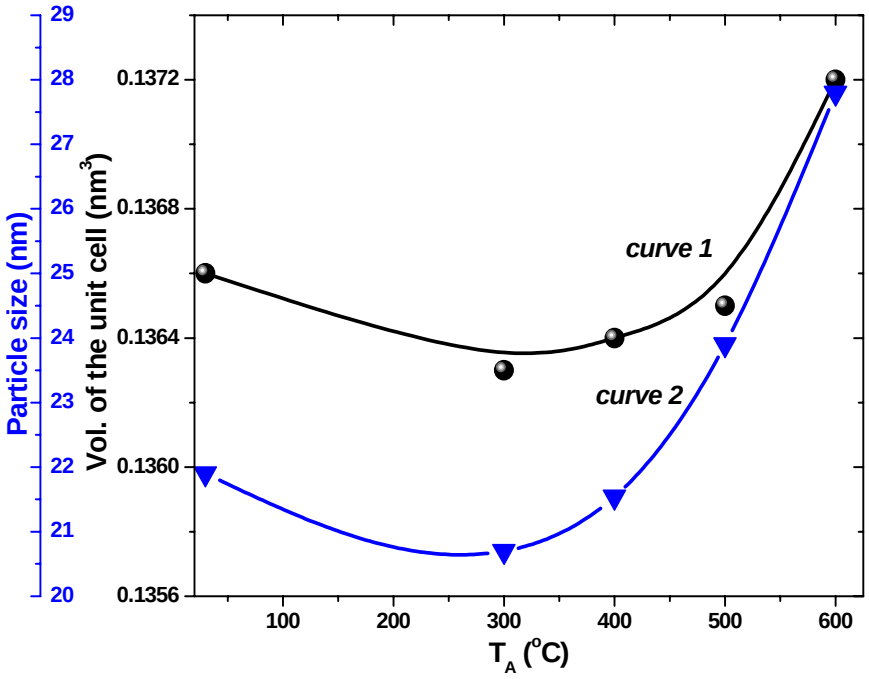
Particle size (nm)
Vol. of the unit cell (nm3)
curve 1
curve 2
0.1372
0.1368
0.1364
0.1360
0.1356
29
28
27
26
25
24
23
22
21
20
100
200
300
400
500
600
TA (°C)

Fig. 3

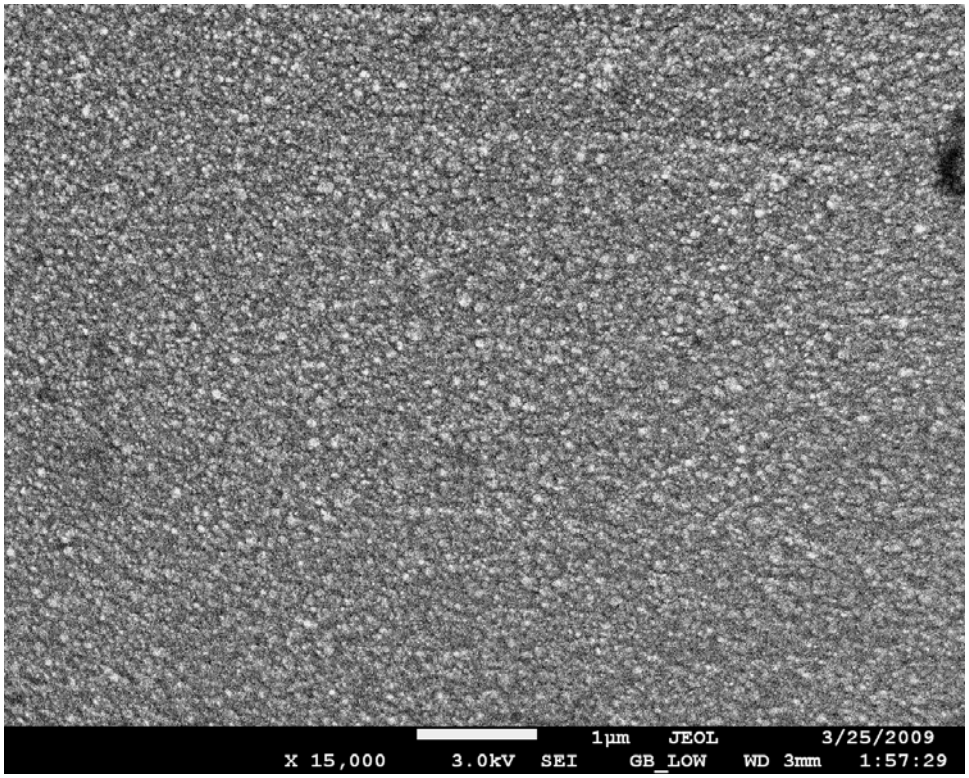
1μm JEOL 3/25/2009
X 15,000 3.0kV SEI GB_LOW WD 3mm 1:57:29

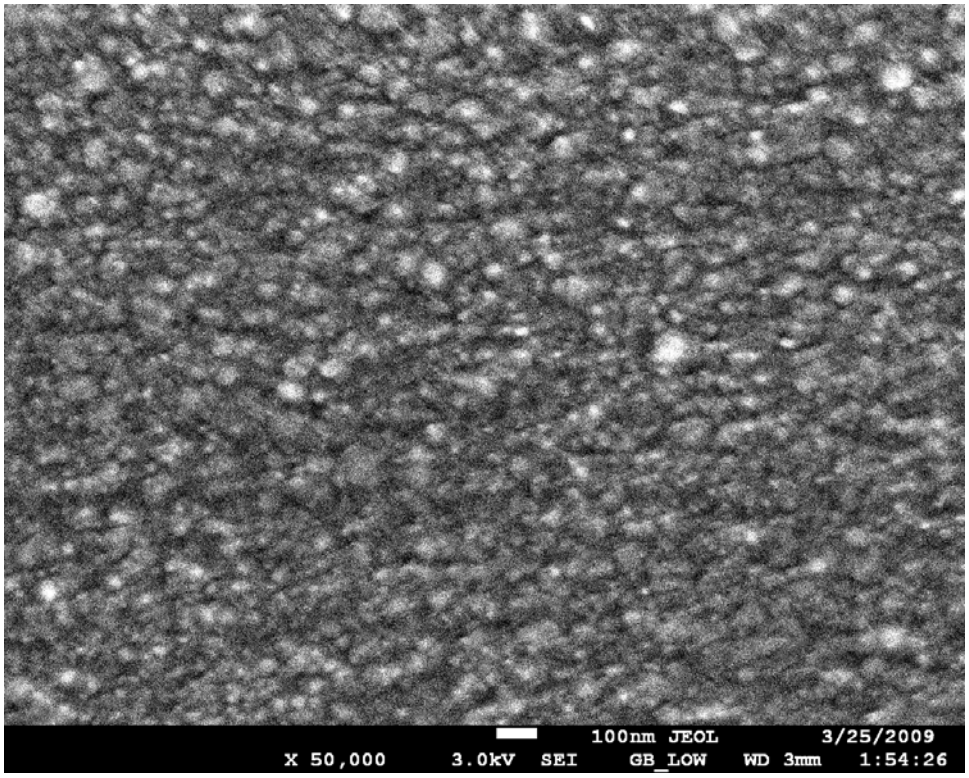
100nm JEOL 3/25/2009
X 50,000 3.0kV SEI GB_LOW WD 3mm 1:54:26

Fig. 4

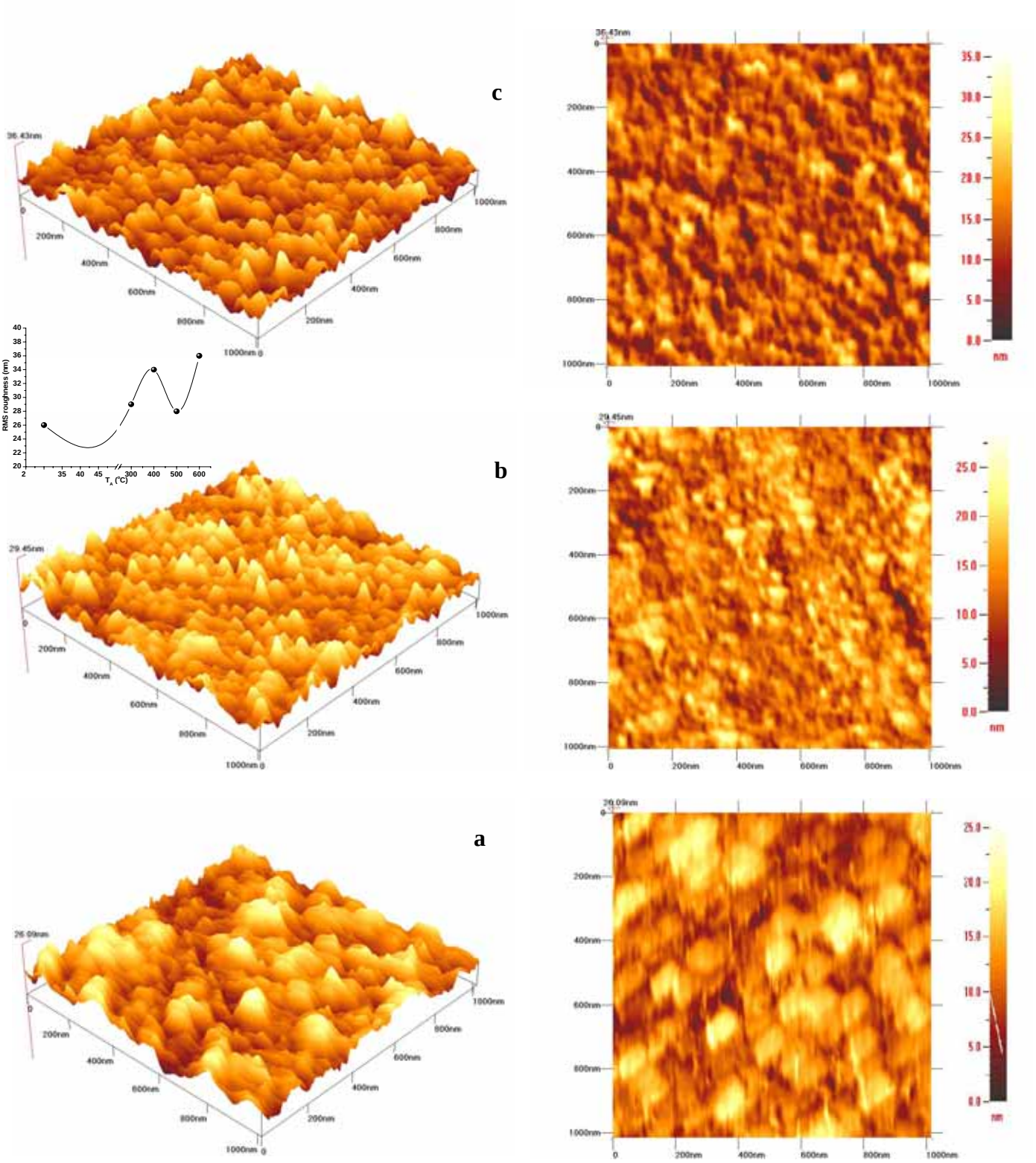

Fig. 5

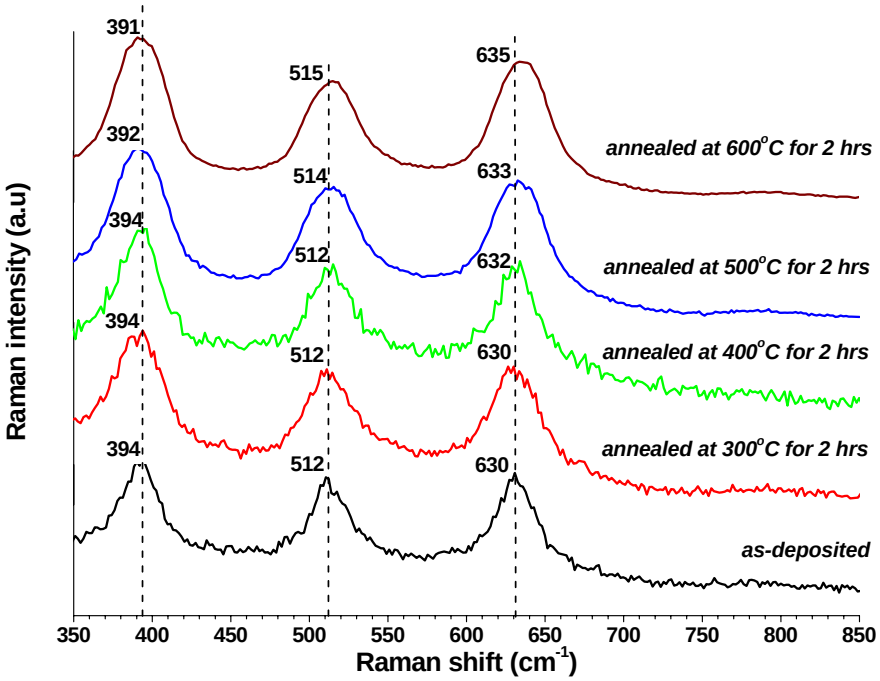
391
515
635
392
annealed at 600°C for 2 hrs
514
633
394
annealed at 500°C for 2 hrs
512
632
394
annealed at 400°C for 2 hrs
512
630
394
annealed at 300°C for 2 hrs
512
630
as-deposited
Raman intensity (a.u)
350
400
450
500
550
600
650
700
750
800
850
Raman shift (cm-1)

Fig. 6

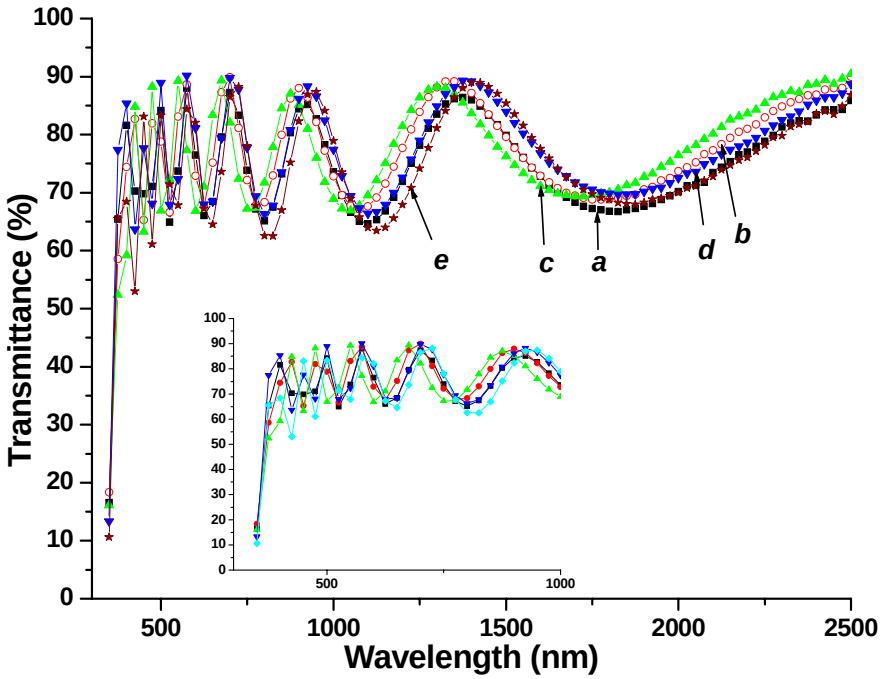
Transmittance (%)
Wavelength (nm)
0
10
20
30
40
50
60
70
80
90
100
500
1000
1500
2000
2500
e
c
a
d
b

Fig. 7

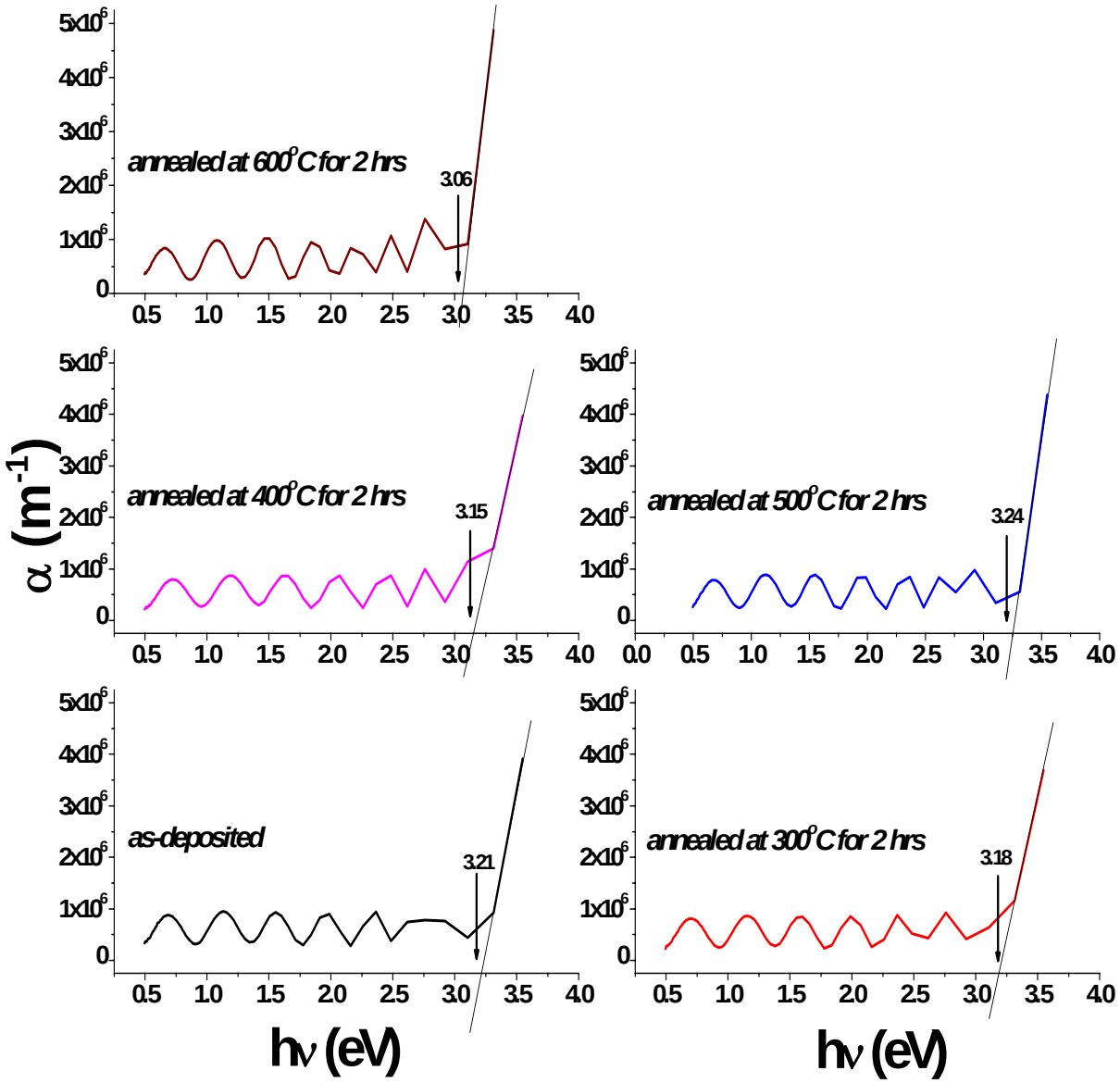
α (m-1)
annealed at 600°C for 2 hrs
3.06
annealed at 400°C for 2 hrs
3.15
annealed at 500°C for 2 hrs
3.24
as-deposited
3.21
annealed at 300°C for 2 hrs
3.18
hν (eV)
hν (eV)

Fig. 8

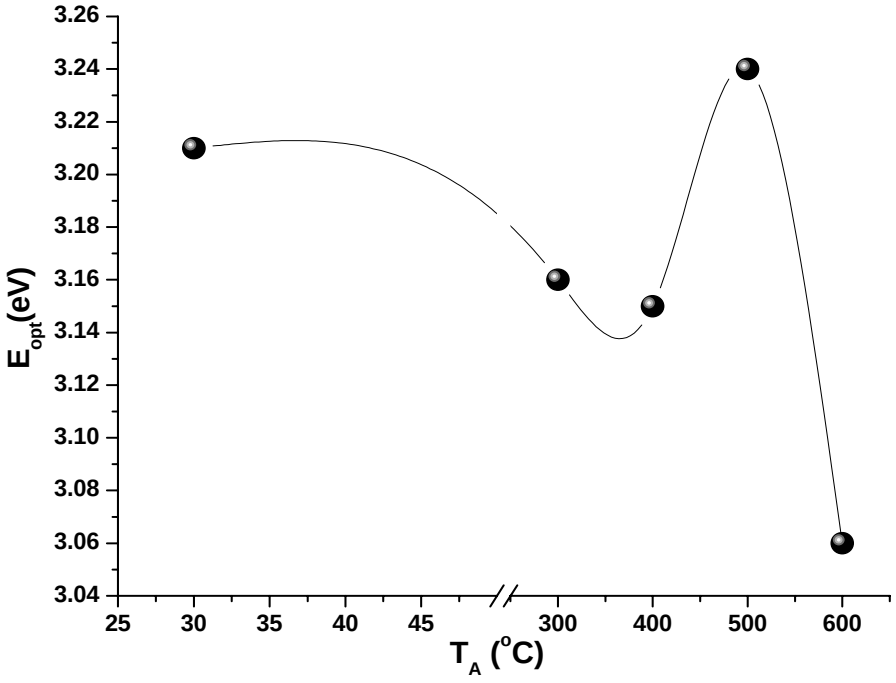
3.26
3.24
3.22
3.20
3.18
3.16
3.14
3.12
3.10
3.08
3.06
3.04
E_{opt}(eV)
25
30
35
40
45
300
400
500
600
T_A (^oC)

Fig. 9

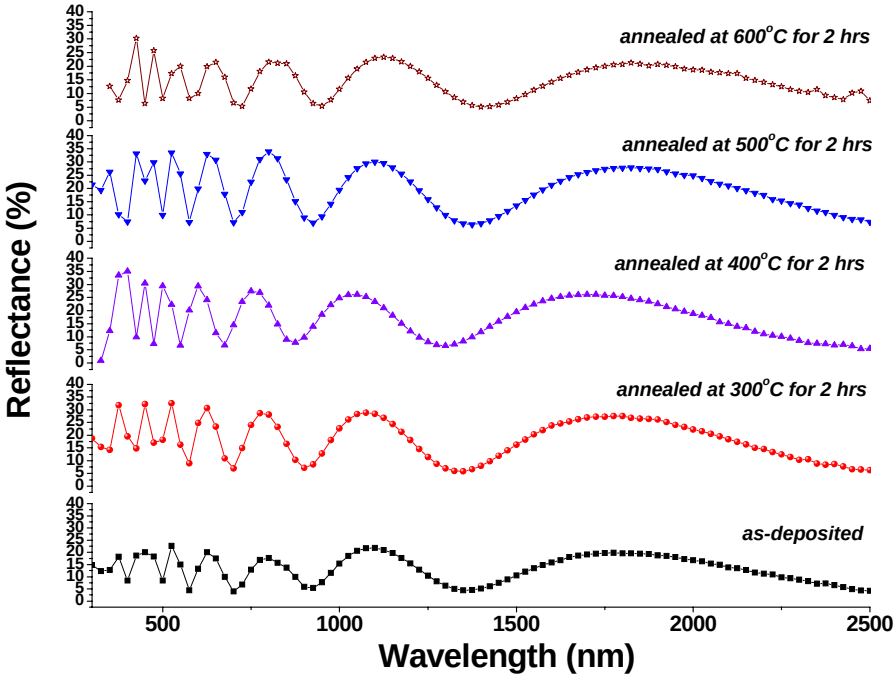
annealed at 600°C for 2 hrs
annealed at 500°C for 2 hrs
annealed at 400°C for 2 hrs
annealed at 300°C for 2 hrs
as-deposited
Reflectance (%)
500
1000
1500
2000
2500
Wavelength (nm)

Fig. 10

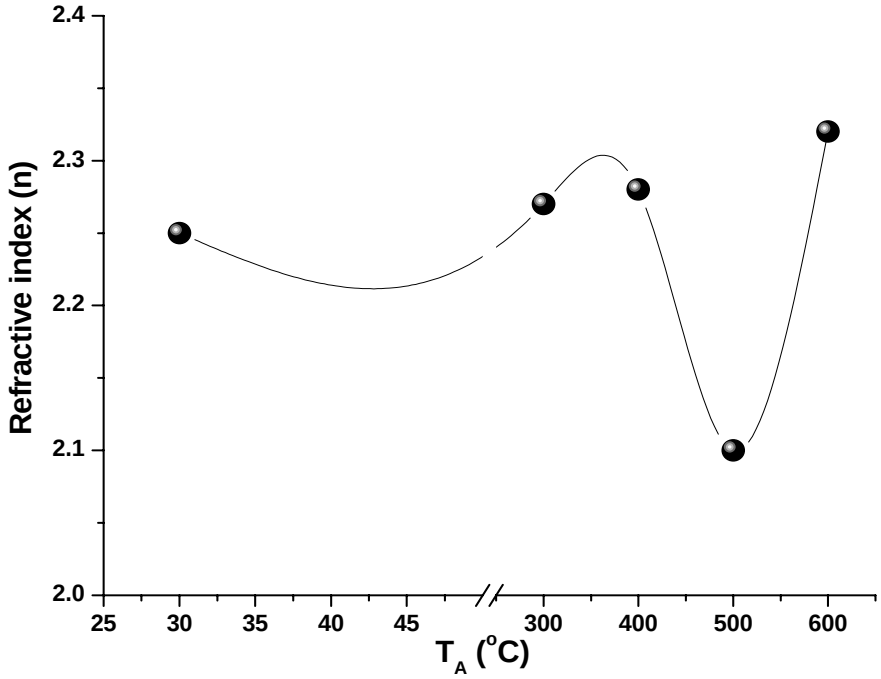
Refractive index (n)
2.4
2.3
2.2
2.1
2.0
25
30
35
40
45
300
400
500
600
T_A (°C)

Fig. 11

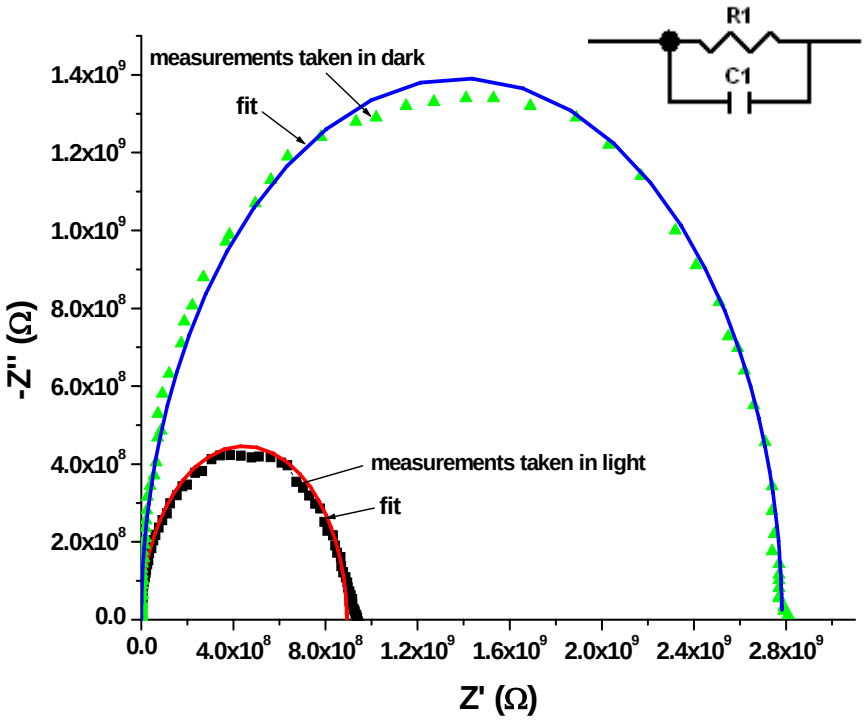
R1
C1
measurements taken in dark
fit
measurements taken in light
fit
-Z'' (Ω)
1.4x10^9
1.2x10^9
1.0x10^9
8.0x10^8
6.0x10^8
4.0x10^8
2.0x10^8
0.0
0.0
4.0x10^8
8.0x10^8
1.2x10^9
1.6x10^9
2.0x10^9
2.4x10^9
2.8x10^9
Z' (Ω)

Fig. 12

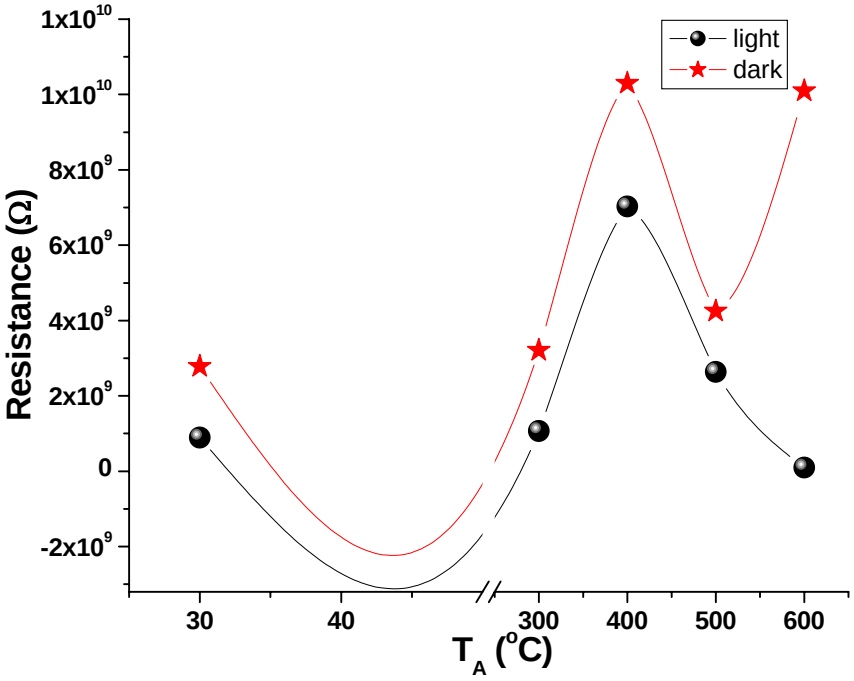
1x10^10
1x10^10
8x10^9
6x10^9
4x10^9
2x10^9
0
-2x10^9
Resistance (Ω)
light
dark
30
40
300
400
500
600
T_A (°C)